

# Thin films of van der Waals fluid: From interface interactions to wetting transitions

Arik Yochelis<sup>a,\*</sup>, Len M. Pismen<sup>b</sup>

<sup>a</sup> Department of Chemical Engineering, Technion – Israel Institute of Technology, 32000 Haifa, Israel

<sup>b</sup> Department of Chemical Engineering and Minerva Center for Nonlinear Physics of Complex Systems, Technion – Israel Institute of Technology, 32000 Haifa, Israel

Received 14 March 2005; received in revised form 19 August 2005; accepted 30 August 2005

Available online 13 October 2005

## Abstract

We present a theoretical study of wetting phenomena and interactions between liquid–vapor interfaces based on the local density functional theory. The focus is mostly on the impact of long-range van der Waals interactions both within the fluid and between the fluid and substrate. For the latter, we consider two models – hard wall and soft wall approximations – differing by the role of steric effects and leading to a qualitatively different character of phase transitions. We compute numerically the disjoining and conjoining potentials (which are important dynamically for spreading, spinodal dewetting, and coarsening in thin films, as well as resolution of interfacial singularities), and loci of intermediate and complete wetting transitions as functions of the Hamaker constant and temperature. We find that taking into account short-range interactions is essential for the description of wetting transitions in the soft wall limit. We derive an analytical form of the disjoining potential and analyze it in the context of the complete, frustrated and partial wetting.

© 2004 Elsevier B.V. All rights reserved.

**Keywords:** Thin film; Disjoining potential; Precursor layer; Wetting

## 1. Introduction

Recent studies of dynamic behavior of thin liquid films and three-phase contact lines showed the crucial role of precursor layers in contact line dynamics and droplet interaction in the course of spinodal dewetting and coarsening [1–3]. While the role of precursor layers in wetting and spreading phenomena had been discussed for a long time [4], only recently it was realized that the motion of contact lines is strongly influenced by the precursor layers even when the liquid is not completely wetting [1,5].

*Intermediate* wetting transitions leading to the formation of mesoscopic fluid layers, as distinct from *complete* wetting when a macroscopic layer is formed, were discovered long time ago [6–9], and observed recently experimentally on solid [10] and liquid [11–15] substrates. Both complete and intermediate wetting transitions are assumed to incorporate both short and long-

range interactions. However, a well formulated theoretical study which justifies the individual impact of such interactions is still missing, though it is recognized as a prime theoretical subject of interest in view of recent experimental observations and their partial agreement with available phenomenological models [16].

The mesoscopic dynamic diffuse interface theory [1,2] uses the wide separation between the width of mesoscopic layers and the scale of hydrodynamic motion to reduce the hydrodynamic equations to a generalized Cahn–Hilliard equation where the disjoining potential of the fluid layer [17] serves as the driving force of the fluid motion along the film. A similar approach applied to a mesoscopic layer separating two identical bulk fluid phases can be used for the description of coalescence dynamics, and has been recently discussed in connection to resolving an interfacial singularity in viscous flow [20]. Another problem where this technique is relevant is film stability and resolution of a singularity arising during nucleation of holes [18,19].

The cited works used model expressions for the disjoining potential obtained in the sharp interface approximation, while emphasizing the essential role of the diffuse character of the vapor–liquid interface (known already to van der Waals [21]) for resolving the interfacial singularities. The dynamic importance of the disjoining potential in mesoscopic lay-

\* Corresponding author. Present address: Department of Physics, University of California at Berkeley, Berkeley, CA 94720-7300, USA. Tel.: +1 510 6433350; fax: +1 510 6438497.

E-mail address: [yochelis@berkeley.edu](mailto:yochelis@berkeley.edu) (A. Yochelis).

ers necessitates, however, precise computation linking it to molecular interactions in the fluid and between the fluid and substrate. The adequate tool for these computations is density functional theory (DFT) [22]; further reduction to a local (van der Waals–Landau–Cahn) theory through small gradient expansion is invalid when the interaction is long-range (i.e. has a power decay) [23]. The original local DFT turned out to be inadequate for the description of fluid layering near interfaces, and various nonlocal theories involving coarse-grained densities have been suggested, including the density-weighted procedure [24] and density-dependent weighting [25]. Application of these methods necessitates heavy numerical computations. Numerical DFT computations were carried out in the context of phenomenological phase transition studies [6,26] without emphasis on computation of disjoining potential.

In this communication, we explore this problem anew using the simplest long-range interaction potential, which allows for a direct link between the wetting properties and thermodynamics of a van der Waals fluid. We pay special attention to the character of interactions in the vicinity of the substrate, and explore limiting cases of “hard wall” and “soft wall” interactions. The first version used in earlier computations [26] exaggerates steric density depletion near the substrate, and the opposite limit may be more relevant for rough solid interfaces, as well as for films on liquid substrates.

Exploration of these limits can be seen as a semi-quantitative alternative to heavy computations in the framework of nonlocal DFT, which are particularly difficult in the wetting context when the vapor–liquid and liquid–solid interfaces closely approach one the other both near the three-phase contact line and in the precursor film. In the two limiting cases we consider, the computations can be carried out analytically, thereby delineating limiting types of behavior near the wetting transition. We apply the same approach to interacting vapor–liquid interfaces near an interfacial singularity.

The character of wetting transitions interactions, as well as properties of the precursor layer, are very much different in both limits. It was found that the analysis in the soft wall approximation based solely on van der Waals disagrees with results of recent experiments on binary fluid systems [11–15]. We included therefore a weak dependence on short-range interactions; the expression for the disjoining potential modified in this way was found to be in a good qualitative agreement with the experiment.

## 2. Density functional equations

Our starting point is the free energy functional written in the local density functional approximation [29] as:

$$\mathcal{F} = \int \rho(\mathbf{r}) f[\rho(\mathbf{r})] d^3\mathbf{r} + \frac{1}{2} \int \rho(\mathbf{r}) d^3\mathbf{r} \int_{r'>d} U(r') [\rho(\mathbf{r} + \mathbf{r}') - \rho(\mathbf{r})] d^3\mathbf{r}', \quad (1)$$

where  $f(\rho)$  is free energy per particle of a homogeneous fluid and  $U(r')$  is an isotropic pair interaction kernel with a short-scale cut-off  $d$ . The functional (1) is written in the form [30] separating

the contribution of density inhomogeneities, expressed by the last term vanishing in a homogeneous fluid, but is equivalent to an alternative form used in earlier works [23].

The chemical potential  $\mu = \delta\mathcal{F}/\delta\rho$  enters the respective Euler–Lagrange equation obtained by minimizing the grand ensemble thermodynamic potential  $\Phi = \mathcal{F} - \mu \int \rho d^3\mathbf{r}$ , which defines the equilibrium density distribution  $\rho(\mathbf{r})$ :

$$g(\rho) - \mu + \int_{r'>d} U(r') [\rho(\mathbf{r} + \mathbf{r}') - \rho(\mathbf{r})] d^3\mathbf{r}' = 0, \quad (2)$$

where  $g(\rho) = d[\rho f(\rho)]/d\rho$ . The function  $F(\rho) = \rho[f(\rho) - \mu]$  should have two minima  $\rho^\pm$  corresponding to two stable uniform equilibrium states of higher and lower density (liquid and vapor).

A simple example of long-range potential is the modified Lennard–Jones potential with hard-core repulsion:

$$U = \begin{cases} -C_W r^{-6} & \text{at } r > d \\ \infty & \text{at } r < d \end{cases}, \quad (3)$$

where  $d$  is the nominal hard-core molecular diameter. The interaction kernel  $U(r)$  gives the free energy density of a homogeneous van der Waals fluid [30]:

$$f(\rho, T) = T \ln \frac{\rho}{1 - b\rho} - a\rho, \quad (4)$$

where  $T$  is temperature,  $b = 2/3\pi d^3$  is the excluded volume and

$$a = -2\pi \int_d^\infty U(r) r^2 dr = \frac{2\pi C_W}{3d^3}. \quad (5)$$

Equilibrium between the two homogeneous states,  $\rho = \rho_0^\pm$  is fixed by the Maxwell condition:

$$\mu_0 = \frac{\rho_0^+ f(\rho_0^+) - \rho_0^- f(\rho_0^-)}{\rho_0^+ - \rho_0^-}, \quad (6)$$

which defines, together with  $\mu_0 = g(\rho_0^\pm)$ , the equilibrium chemical potential  $\mu = \mu_0$  and both equilibrium densities.

The equation for the density distribution near a flat boundary normal to the  $z$ -axis is obtained by assuming  $\rho$  to be constant in each lateral plane and integrating Eq. (1) in the lateral directions. This yields the free energy per unit area, or surface tension:

$$\gamma = \int_{-\infty}^\infty \rho(z) [f(\rho) - \mu] dz + \frac{1}{2} \int_{-\infty}^\infty \rho(z) dz \int_{-\infty}^\infty Q(\zeta) [\rho(z + \zeta) - \rho(z)] d\zeta. \quad (7)$$

The interfacial energy is contributed both by deviations from the equilibrium density levels in the transitional region and by the distortion energy localized there. The 1D interaction kernel  $Q(z)$  lumps intermolecular interaction between the layers  $z = \text{const}$ . It is computed by lateral integration using as an integration variable the squared distance  $q = r^2 = \xi^2 + z^2$ , where  $\xi$  is radial distance in the lateral plane. Taking note that the lower integration limit for  $q$  is  $q_0 = z^2$  at  $|z| > d$ ,  $q_0 = d^2$  at  $|z| \leq d$ , we compute:

$$Q(z) = -\pi C_W \int_{q_0}^\infty q^{-3} dq = \begin{cases} -\frac{1}{2}\pi C_W z^{-4} & \text{at } |z| > d \\ -\frac{1}{2}\pi C_W d^{-4} & \text{at } |z| \leq d. \end{cases} \quad (8)$$

The respective 1D Euler–Lagrange equation, replacing Eq. (2), is:

$$g[\rho(z)] - \mu + \int_{-\infty}^{\infty} Q(\zeta)[\rho(z + \zeta) - \rho(z)] d\zeta = 0. \quad (9)$$

This equation can be rewritten in a dimensionless form:

$$g(\rho) - \mu + \frac{3}{4}\beta \int_{-\infty}^{\infty} Q(\zeta)[\rho(z + \zeta) - \rho(z)] d\zeta = 0, \quad (10)$$

where:

$$g(\rho) = \frac{1}{1 - \rho} - \ln\left(\frac{1}{\rho} - 1\right) - 2\beta\rho. \quad (11)$$

Here the length is scaled by the nominal molecular diameter  $d$ , the density by  $b^{-1}$ , and the chemical potential by  $T$ ; the interaction kernel is  $Q(z) = -z^{-4}$  at  $|z| > 1$ ,  $Q(z) = -1$  at  $|z| \leq 1$ , and the only remaining dimensionless parameter is the rescaled inverse temperature  $\beta = a/(bT)$ .

An example of a density profile obtained by solving numerically Eq. (10) is shown in Fig. 1. The density tail asymptotics can be estimated by considering a location far removed from the interface placed at the origin [ $|z| \gg 1$  in the dimensionless units of Eq. (10)] where a sharp interface limit can be implemented. The density is presented as  $\rho = \rho_0^\pm + \tilde{\rho}$ , where  $\tilde{\rho}/\rho \sim 1/|z|^3 \ll 1$ . Inserting this in (11) and linearizing around  $\rho = \rho_0^\pm$ , we see that the densities inside the integral are well approximated in the leading order by the two limiting constants, which is equivalent to the sharp interface limit. For example, for the vapor tail at  $z > 0$ ,  $|z| \gg 1$ , we have  $\rho(z) = \rho_0^-$  and  $\rho(z + \zeta) = \rho_0^+$  for  $\zeta > |z|$ ,  $\rho(z + \zeta) = \rho_0^-$  for  $\zeta < |z|$ . Thus, we obtain

$$\rho = \rho_0^\pm + \frac{\beta(\rho_0^+ - \rho_0^-)}{4g'(\rho_0^\pm)} \frac{1}{z^3}. \quad (12)$$

This is in good agreement to the numerical solution, as seen in the inset of Fig. 1. One can check a posteriori using this expression that the contribution to the integral of neighboring locations with

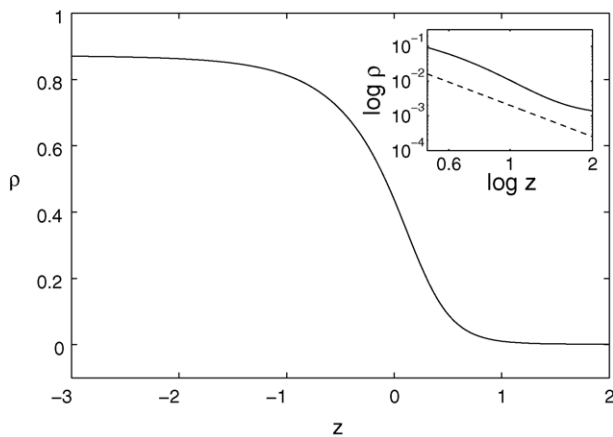


Fig. 1. The density profile of the liquid–vapor interface at  $\beta = 9$  obtained by numerical solution of (10). The inset shows the vapor-phase tail of the numerical solution (solid line) compared to the asymptotic form (12) depicted by the dashed line.

$|\zeta| = O(1)$  is of a higher order  $\propto |z|^{-5}$  and therefore can be neglected.

### 3. Interacting liquid–vapor interfaces

If two flat liquid–vapor interfaces are in close proximity, the equilibrium chemical potential and surface tension become dependent on their mutual separation  $h$ . This phenomenon is relevant for processes of topology change, e.g. droplet coalescence. The corrections due to proximity of interfaces in the case when a gas layer separates two identical semi-infinite bulk liquids can be obtained by finding a homoclinic solution of Eq. (10) satisfying the asymptotic conditions  $\rho(\pm\infty) = \rho^\pm$ . A stationary solution of such kind exists at certain values of  $\mu$  shifted downwards from the Maxwell construction level  $\mu_0$ . The shift  $\Delta\mu_c = \mu_0 - \mu$  corresponds to the *conjoining potential* expressing the interaction of two identical flat interfaces.

A rough but qualitatively correct approximation can be obtained by computing molecular interactions between two sharp interfaces [20]. The shift of chemical potential necessary to keep two interfaces separated by a distance  $h$  in the state of equilibrium is determined in this approximation by the decrement of the integral in Eq. (10) due to replacing gas by liquid at  $z > h$ . For the purpose of a qualitative estimate, the sharp interface computation valid at  $h \gg 1$  can be extended also to small separations, ( $h \leq 1$ ) to find [20]:

$$\Delta\mu_c = \begin{cases} \frac{4}{3} - h & \text{at } h \leq 1, \\ \frac{1}{3}h^{-3} & \text{at } h > 1, \end{cases} \quad (13)$$

Equilibrium of a layer between two interfaces is unstable; the instability is, however, very weak when separation of interfaces is large compared to the molecular scale. Localized small perturbations decay under these conditions due to surface tension, and a large disturbance is needed to create a critical nucleus initiating the topology change.

A precise dependence is obtained by solving numerically Eq. (10). The solution is found by fixing some trial value of  $\mu$  and solving Eq. (10) iteratively to find a stationary profile  $\rho(z)$  at this value. The nominal gap width is defined as:

$$h = \frac{1}{\rho^+ - \rho^-} \int_{-\infty}^{\infty} (\rho^+ - \rho) dz. \quad (14)$$

The computation results for  $\beta = 9$  are shown by dots in Fig. 2. The curve  $\Delta\mu_c(h)$  expressing this dependence well fits the computational results shifted by a certain value  $h_*$ , equal to  $\approx 1.39$  in this particular computation. A shift is necessary because, while the separation in Eq. (13) can be formally arbitrarily small, no stationary solution of Eq. (10) can exist below a certain value of  $h$  which corresponds to a critical size required for nucleation of a critical 1D “bubble”. The applied shift equals to the width of this “bubble” computed according to Eq. (14).

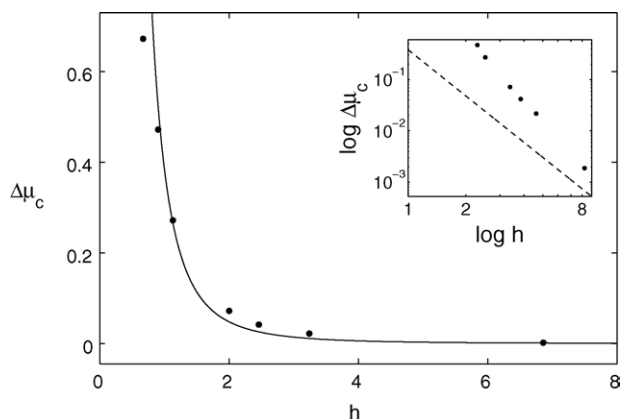


Fig. 2. The dependence of the dimensionless conjoining potential  $\Delta\mu_c$  on separation  $h$ . The dots denote the results of 1D density functional computation with a shift of  $h_* = 1.39$  adjusted to fit Eq. (13), as shown by the solid line. Inset: the tail of the numerical dependence  $\Delta\mu_c(h)$  compared to the  $h^{-3}$  decay (dashed line).

### 4. Fluid–substrate interactions

#### 4.1. Disjoining potential

In the proximity of a substrate surface, the additional term in the free energy integral (1) is:

$$\mathcal{F}_s = \int \rho(\mathbf{r}) d^3\mathbf{r} \int U_s(|r - r'|) \rho_s(\mathbf{r}') d^3\mathbf{r}', \quad (15)$$

where  $U_s$  is the attractive part of the fluid–substrate interaction potential,  $\rho_s$  is the substrate density, and  $\int_s$  means that the integration is carried over the volume occupied by the substrate; all other integrals here and in (1) are now restricted to the volume occupied by the fluid.

In the following, we shall consider a flat interface parallel to the substrate surface  $z = 0$ , and suppose that liquid–substrate interactions are also of the van der Waals type with a modified constant  $C_S = \alpha_s C_W$ . Then the free energy per unit area is expressed, after some rearrangements, as:

$$\gamma_s = \int_0^\infty \rho(z) \left\{ f(\rho) + \psi_l(z) \left[ \alpha_s \rho_s - \frac{1}{2} \rho(z) \right] \right\} dz + \frac{1}{2} \int_0^\infty \rho(z) dz \int_0^\infty Q(z - \zeta) [\rho(\zeta) - \rho(z)] d\zeta. \quad (16)$$

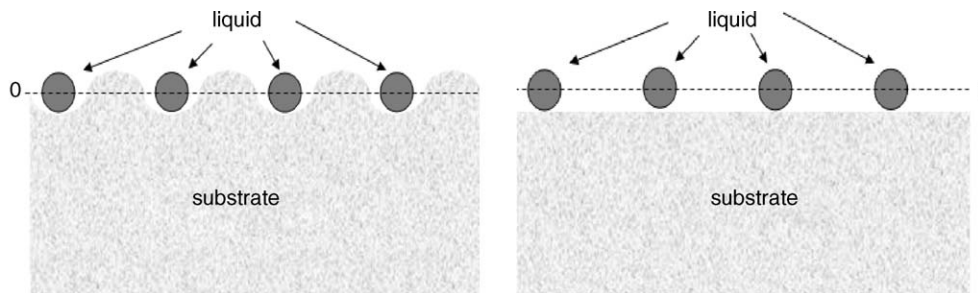


Fig. 3. Schematic cartoon representation of soft (left) and hard (right) wall approximations. Solid circles represent hard sphere fluid molecules and the horizontal coordinate, in this setup is  $z$ .

The first term contains the same local part as in Eq. (7) complemented by the liquid–substrate interaction energy. The latter is computed by integrating the attracting part of the fluid–fluid and fluid–substrate interaction energy laterally as in Eq. (8) and represents the shift of energy compared to the unbounded fluid. The term  $\rho(z)/2$  compensates lost fluid–fluid interactions in the substrate domain which are included in the homogeneous part  $f(\rho)$ .

Computation of the function  $\psi_l(z)$  depends on steric constraints imposed upon fluid molecules in the vicinity of the substrate. We consider two limiting cases, as demonstrated in Fig. 3:

- (i) *Soft wall approximation* (SWA) which allows for fluid molecules to penetrate up to the surface of the substrate.
- (ii) *Hard wall approximation* (HWA) which imposes steric constraints preventing the centers of fluid molecules from approaching the substrate at distances shorter than the hard-core cut-off  $d$  or 1 in dimensionless units.

To be definite, we place the origin of the coordinate system on the centerline of the first row of the substrate atoms. In the soft wall approximation, the computation yields:

$$\psi_l(z) = -\pi C_W \int_{-\infty}^0 d\zeta \int_{q_0}^\infty q^{-3} dq = \int_{-\infty}^0 Q(z - \zeta) d\zeta, \quad (17)$$

where the integration limit is  $q_0 = (z - \zeta)^2$  at  $|z - \zeta| > d$ ,  $q_0 = d^2$  at  $|z - \zeta| \leq d$ . The result is:

$$\psi_l(z) = \begin{cases} -\frac{1}{6} \pi C_W z^{-3} & \text{at } |z| > d \\ -\pi C_W d^{-3} \left( \frac{2}{3} - \frac{z}{2d} \right) & \text{at } |z| \leq d. \end{cases} \quad (18)$$

The dimensionless Euler–Lagrange equation derived from Eq. (16) reads:

$$g(\rho) - \mu + \frac{3}{4} \beta \psi_l(z) [\rho^+(\chi + 1) - \rho(z)] + \frac{3}{4} \beta \int_0^\infty Q(\zeta - z) [\rho(\zeta) - \rho(z)] d\zeta = 0 \quad (19)$$

where  $\chi = \alpha_s \rho_s / \rho^+ - 1$  is the dimensionless Hamaker constant, and  $\psi_l(z) = -z^{-3}/3$  at  $z > 1$ ,  $\psi_l(z) = z - 4/3$  at  $z \leq 1$ .

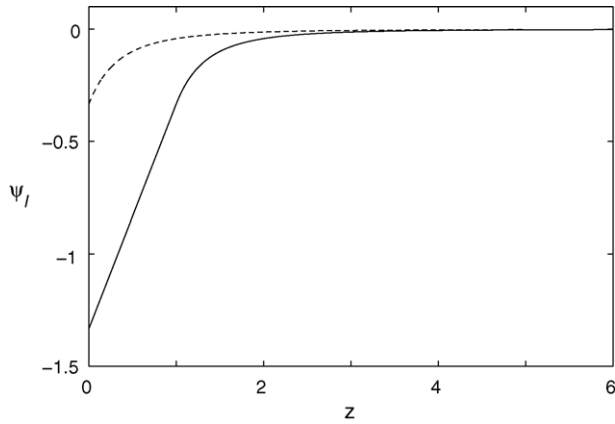


Fig. 4. The function  $\psi_l(z)$  for soft (solid line) and hard (dashed line) wall approximations.

The hard wall approximation introduces, in effect, a void layer with the thickness equal to the hard-core cut-off; hence,  $\psi_l(z) = 0$  at  $0 < z \leq 1$  [26]. If the closest allowed position of the centers of fluid molecules is taken as the origin, then we define a hard wall fluid–substrate interaction as  $\psi_l^{\text{HWA}}(z) = \psi_l^{\text{SWA}}(z + 1)$  as seen in Fig 4. This shift significantly changes the equilibrium solution and the character of the wetting transition.

The equilibrium chemical potential is shifted from the Maxwell construction,  $\mu = \mu_0$  in the proximity of the substrate surface. The shift  $\Delta\mu_d = \mu - \mu_0$ , called *disjoining potential* [17], can be defined as:

$$\Delta\mu_d = \frac{1}{\rho_0^+ - \rho_0^-} \frac{\partial \gamma_s}{\partial h}, \tag{20}$$

where  $h$  is the nominal distance between gas–liquid and liquid–substrate interfaces. The latter is defined, analogous to Eq. (14), as:

$$h = \frac{1}{\rho^+ - \rho^-} \int_0^\infty (\rho - \rho^-) dz. \tag{21}$$

### 4.2. Equilibrium solutions

The sign of  $\chi$  distinguishes a perfectly wetting fluid at  $\chi > 0$  and a “nonwetting” fluid forming a finite contact angle at  $\chi < 0$ . In the latter case, there are two branches of equilibrium solutions of Eq. (19) parametrized by the disjoining potential  $\Delta\mu_d$ . The stable branch with small  $h$  is characterized by a monotonic density profile and corresponds to the vapor-phase thickening to a relatively dense adsorbate or precursor layer near the substrate. The unstable branch with larger  $h$  is characterized by a non-monotonic density profile and corresponds to a liquid layer with a slightly depleted density near the substrate. Instability is characteristic to any layer of a nonwetting fluid, but it is very weak when separation of the vapor–liquid and liquid–substrate interfaces is large compared to the molecular scale. The contact angle can be expressed through the disjoining potential for the case  $|\chi| \ll 1$  when a small-angle approximation is valid [30]:

$$\theta = \sqrt{\frac{2\rho^+}{\gamma} \int_{h_0}^\infty \Delta\mu_d dh}, \tag{22}$$

where  $h = h_0$  is the precursor layer thickness defined by the condition  $\mu(h_0) = \mu_0$  or  $\Delta\mu_d(h_0) = 0$ .

Figs. 5(a) and 6(a) present typical equilibrium curves  $\Delta\mu_d(h)$ , respectively, for the SWA and HWA. Examples of the corresponding density profiles are shown in Figs. 5(b) and 6(b). One should keep in mind that in the hard wall approximation,  $h$  should be rescaled back so that the density profiles start at  $h = 1$ . Unlike in the soft wall approximation, in the hard wall case, the void between the substrate and the liquid density encourages density depletions (see inset of Fig. 6(b)). All solutions exhibit a  $\Delta\mu_d \sim h^{-3}$  tail at large  $h$ , in agreement to calculations performed in the sharp interface approximation [30]. Oscillatory density tails cannot appear in our model, unlike more sophisticated nonlocal DFT computations [31,26]. Although the curves  $\Delta\mu_d(h)$  are qualitatively similar to those obtained in the sharp interface approximation [30], the quantitative distinctions strongly influence the character of the wetting transition, as will be emphasized in the following.

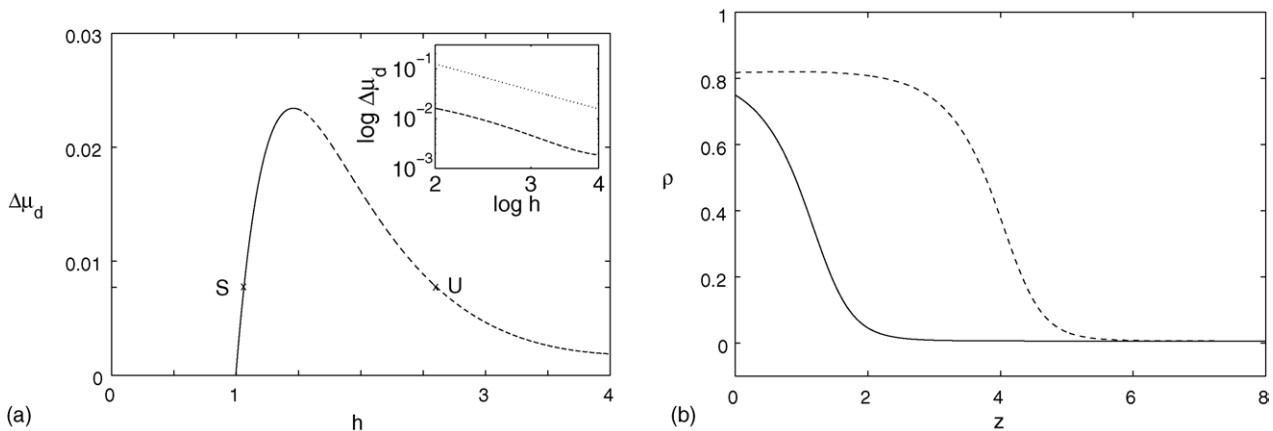


Fig. 5. Equilibrium solutions of Eq. (19) in the soft wall approximation (SWA). (a) The dependence of the dimensionless disjoining potential  $\Delta\mu_d$  on separation  $h$ . The solid/dashed lines denote stable/unstable solutions, respectively. The dotted line in the inset depicts the  $h^{-3}$  decay. (b) Coexisting density profiles at  $\Delta\mu_d = 2.2 \times 10^{-3}$ . Stable (solid line) and unstable (dashed line) profiles correspond to S and U in (a), respectively. Parameters:  $\chi = -0.05$ ,  $\beta = 7$ .

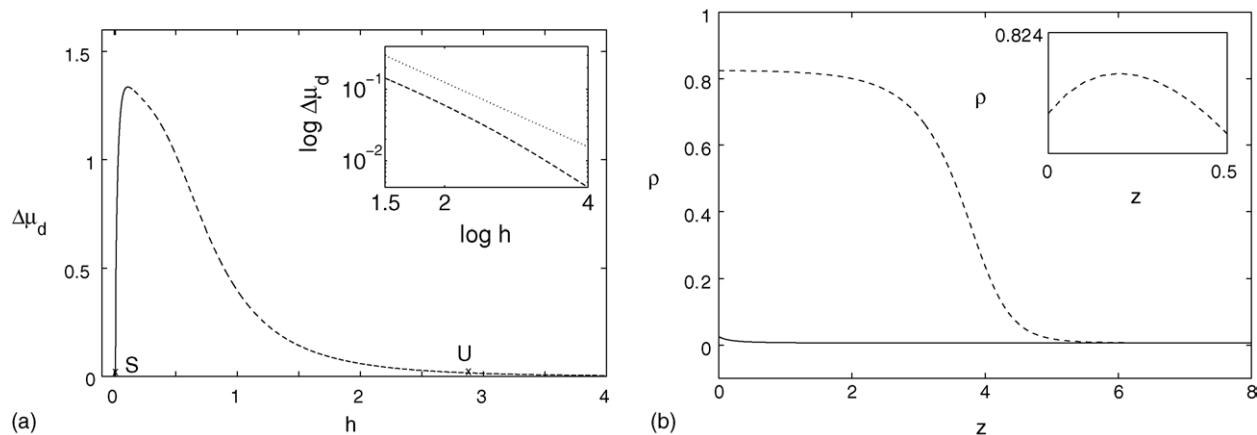


Fig. 6. Equilibrium solutions of Eq. (19) in the hard wall approximation (HWA). (a) The dependence of the dimensionless disjoining potential  $\Delta\mu_d$  on separation  $h$ . The solid/dashed lines denote stable/unstable solutions, respectively. The dotted line in the inset depicts the  $h^{-3}$  decay. (b) Coexisting density profiles at  $\Delta\mu_d = 7.7 \times 10^{-3}$ . Stable (solid line) and unstable (dashed line) profiles correspond to  $S$  and  $U$  in (a), respectively. Parameters:  $\chi = -0.05$ ,  $\beta = 7$ .

### 4.3. Comparison between HWA and SWA

Investigating numerically the two above substrate–liquid interaction models, we can distinguish between two main differences in the interaction properties: the emergence of “microscopic” solutions, identified with nanoscale precursor layers and transition to layers of mesoscopic or macroscopic thickness. The three classes of films correspond, respectively, to  $h \sim \mathcal{O}(1)$ ,  $h \sim \mathcal{O}(10)$ ,  $h > \mathcal{O}(10^2)$  (measured on the molecular scale  $d$ ).

#### 4.3.1. Precursor layer

Stable equilibrium solutions with a finite thickness  $h = h_0$ , which correspond to a microscopic precursor layer, exist at the liquid–vapor equilibrium chemical potential  $\mu = \mu_0$ . An example of the dependence of the dimensionless precursor layer thickness on the inverse temperature  $\beta$  is shown in Fig. 7(a). One can see a strong difference between SWA and HWA results. In the HWA computation, the value of  $h_0$  at the chosen value of the Hamaker constant is much less than unity, unless near the criti-

cal temperature  $\beta = \beta_c \simeq 3.37$ , so that one can speak of a dilute adsorption layer rather than of a proper precursor. This difference stems from an effective increase of the absolute value of the Hamaker constant due to the presence of a dilute layer of steric origin present in HWA.

On the other hand, by fixing the value of  $\beta$  and varying  $\chi$ , one finds that a precursor layer may exist only above a critical value  $\chi > \chi_c^-$ , as shown in Fig. 7(b). When the layer thickness is defined by the integral expression (21), this transition loses a qualitative character, and the value  $\chi_c^-$  can be defined as a point where  $\Delta\mu_d(h_0) = 0$  (see Fig. 8(a)). This happens at  $\chi = \chi_c^-(\beta) = -(1 - \rho^-/\rho^+)$ , so that the lower limit is identical for both models (see Fig. 9). According to the integral formula, negative values are possible, and may appear when fluid–substrate interactions are so weak that the fluid is nonwetting even at vapor densities. Moreover, at  $\chi$  slightly above  $\chi_c^-$ , the topology of the curves  $\Delta\mu_d(h)$  for the HWA model changes: the curve becomes discontinuous, and the microscopic and macroscopic branches of the curve separate, as seen in Fig. 8(a).

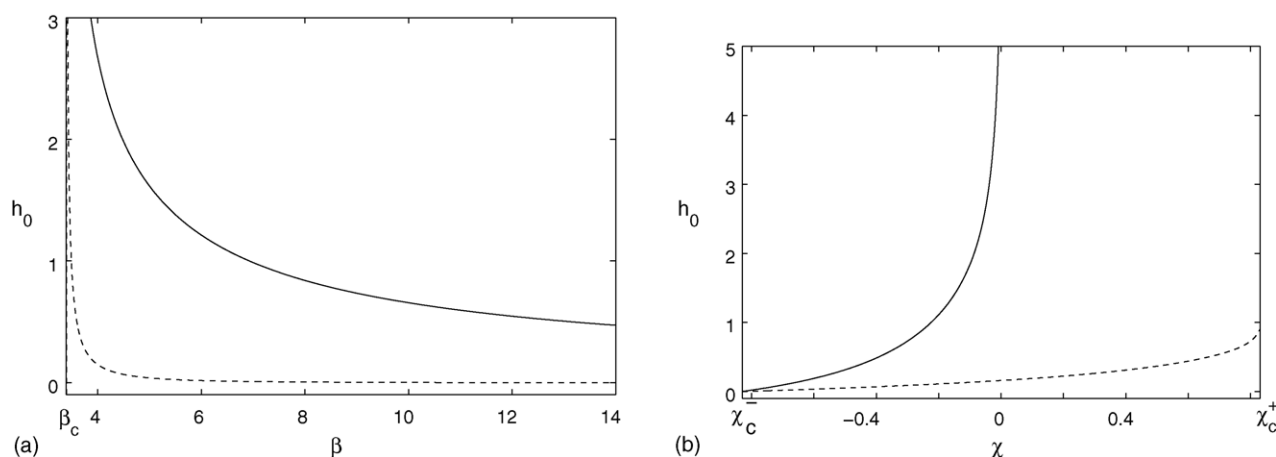


Fig. 7. The dependence of the dimensionless precursor layer thickness on (a) the inverse temperature  $\beta$  for a fixed value of the dimensionless Hamaker constant  $\chi = -0.05$ ; and (b) the Hamaker constant  $\chi$  at  $\beta = 4$ . The solid/dashed lines represent the soft/hard wall approximations, respectively. In (b),  $\chi_c^-$  corresponds to the emergence threshold of the precursor layer, identical in both SWA and HWA models. The precursor thickness at the wetting transition threshold  $\chi = \chi_c^+$  is finite in HWA, indicating a first order transition, while in SWA,  $h_0 \rightarrow \infty$  at  $\chi \rightarrow \chi_c^+ = 0$ , indicating a second order transition.

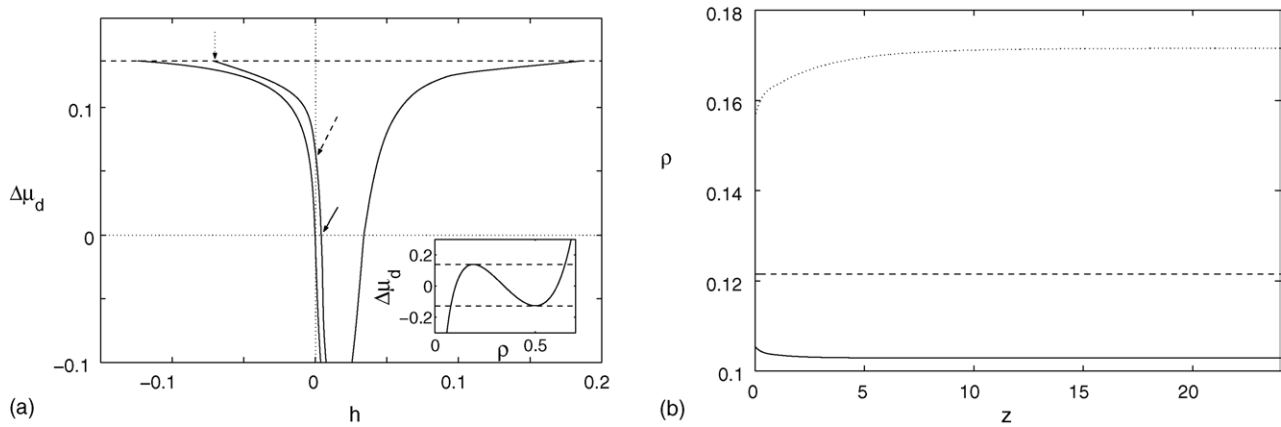


Fig. 8. Equilibrium solutions of Eq. (19) in the hard wall approximation (HWA) in the vicinity  $\chi = \chi_c^- = -0.833$ . (a) The dependence of the dimensionless disjoining potential  $\Delta\mu_d$  on separation  $h$  at  $\beta = 4$  and different values of the Hamaker constant, from right to left,  $\chi = -0.6, -0.8, \chi_c^-$ . The dashed line represents the upper limit of the vapor–liquid coexistence. The coexistence range is demonstrated in the inset. The dashed line denotes the critical shift of chemical potential at which the curve  $\Delta\mu_d(h)$  becomes discontinuous. (b) Density profiles corresponding to the arrows in (a).

The discontinuity is explained by the absence of the vapor–fluid coexistence above some critical value of the chemical potential as shown in the inset of Fig. 8(a). The sequence of density profiles in the vicinity of  $\chi = \chi_c^-$  is shown in Fig. 8(b).

4.3.2. Wetting transitions

A precursor film exists within the interval  $\chi_c^- < \chi < \chi_c^+$ . The latter limit corresponds to the wetting transition, as presented in Fig. 7(b). One can see a qualitative difference between the SWA and the HWA models. For SWA, the precursor thickness grows continuously as  $\chi$  increases, and diverges at  $\chi = \chi_c^+ = 0$ , indicating a second-order transition to complete wetting. For HWA, the precursor layer approaches a finite thickness at finite  $\chi = \chi_c^+$ , indicating a first order transition to wetting. The locus of the wetting transition  $\chi = \chi_c^+(\beta)$  is determined by numerical computation (see Fig. 9).

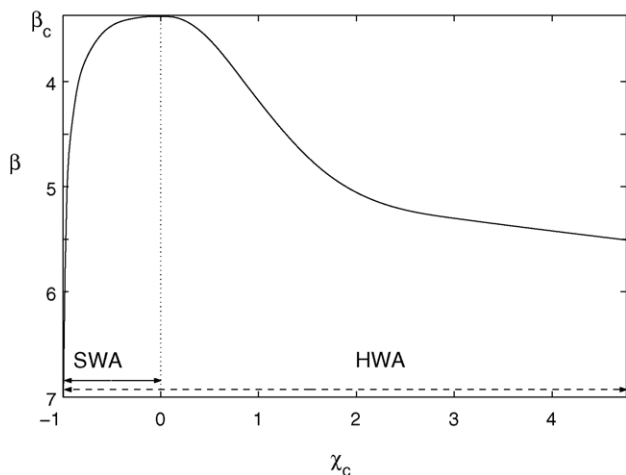


Fig. 9. The dependence of the critical values of the Hamaker constant  $\chi_c$  on inverse temperature  $\beta$  at  $\mu = \mu_0$ . The left branch [ $\chi_c(\beta) < 0$ ] is the limit  $\chi_c^-$  of the emergence of the precursor layer identical for both SWA and HWA models. The right branch [ $\chi_c(\beta) \geq 0$ ] denotes the wetting transition to for HWA. The wetting transition for SWA occurs at  $\chi_c = 0$  independently of  $\beta$ .

The two limiting cases of SWA and HWA correspond to compliant (fluid or rough solid) or molecularly smooth solid substrates, respectively. Recently the transitions of both kind (first and second order) were found in experiments on liquid substrates [15,32]. A disagreement between the SWA results discussed here and in the later experiments is due to the absence of short range interactions in our computations. A more complete picture of wetting transitions in SWA arises when, in addition to long-range interactions, short-range forces between the fluid molecules and the substrate are taken into account [15,16]. While concentrating in the following on short-range interactions in SWA, we refer the reader to reference [26] which describes the impact of short-range interactions in HWA.

4.4. Short-range interactions in SWA

Computation of repulsive short-range interactions in the soft wall approximation takes into account polar interactions. In the simplest description, the interaction kernel for short-range forces has an exponential decay [33,34]:

$$\psi_s = \pi C_p \int_{-\infty}^0 d\zeta \int_{q_0}^{\infty} e^{-\lambda\sqrt{q}} dq, \tag{23}$$

where  $\lambda > 0$ . Some other forms can be also used here [35]. Unlike the computation of  $\psi_l$ , no cut-off is required, and the lower integration limit is  $q_0 = (z - \zeta)^2$ . This yields:

$$\psi_s = \frac{2\pi C_p}{\lambda^3} (2 + \lambda z) e^{-\lambda z}. \tag{24}$$

The modified dimensionless Euler–Lagrange equation reads:

$$g(\rho) - \mu + 3\eta\beta\psi_s(z) + \frac{3}{4}\beta\psi_l(z)[\rho^+(\chi + 1) - \rho(z)] + \frac{3}{4}\beta \int_0^{\infty} Q(\zeta - z)[\rho(\zeta) - \rho(z)] d\zeta = 0 \tag{25}$$

where for simplicity we set  $\lambda = d^{-1}$ ,  $\psi_s(z) = (2 + z) \exp(-z)$  at  $z > 0$  and  $\eta = C_p b^2/a \sim C_p/C_W$ . An analytical form of the

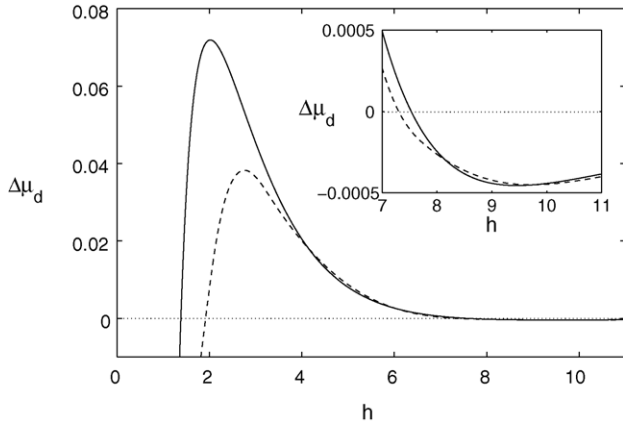


Fig. 10. The dependence of the dimensionless disjoining potential  $\Delta\mu_d$  on separation  $h$ . The solid line denotes the sharp interface approximation form (Eq. (26)) while the direct integration of (25) is demonstrated by the dashed line. Parameters:  $\beta = 9$ ,  $\eta = 0.01$ , and  $\chi = 0.3$ .

disjoining potential can be obtained exploiting the sharp interface approximation for both  $\eta$  and  $\chi \ll 1$ . Adapting the method discussed in [2,30], we find:

$$\Delta\mu_d = \frac{\beta}{4} \left[ 12\eta(2+h)e^{-h} - \rho^+ \frac{\chi}{h^3} - \frac{\rho^+ \beta}{8g'(\rho^+)} \frac{1}{h^6} \right]. \quad (26)$$

The derived analytical form of the disjoining potential (26) is presented in Fig. 10. A comparison with direct numerical integration of (25) shows a good agreement already at  $h < \mathcal{O}(10)$  values.

A qualitative nature of wetting transitions can be captured via a simple analysis of the disjoining potential (26) at the equilibrium chemical potential  $\mu = \mu_0$  and thus  $\Delta\mu_d = 0$ . We distinguish between three characteristic types of behavior which are attributed to the three corresponding wetting regions:

*Complete wetting:* there is a single diverging solution ( $h \rightarrow \infty$ ) at  $\chi > 0$ ,  $\Delta\mu_d = 0$ , which corresponds to a macroscopic layer.

*Frustrated complete wetting:* three solutions exist for  $\chi > 0$ , two of which are finite and the third one is diverging. The two finite solutions have distinct scales, molecular (“microscopic”) and mesoscopic.

*Partial wetting:* two solutions exist for  $\chi < 0$ , where one is finite on a molecular scale and the other one diverges.

The separating boundary between the partial and frustrated complete wetting depends solely on the sign change of the Hamaker constant,  $\chi$ . The transition from frustrated to complete wetting occurs at a certain critical value of  $\eta = \eta_c$  when the maximum of the curve  $\Delta\mu_d(h)$  crosses zero; this happens at a critical thickness  $h = h_c$  defined as:

$$\Delta\mu_d(h_c) = 0, \quad \left. \frac{d\Delta\mu_d}{dh} \right|_{h=h_c} = 0, \quad \left. \frac{d^2\Delta\mu_d}{dh^2} \right|_{h=h_c} < 0. \quad (27)$$

The dependence  $\Delta\mu_d(h)$  at  $\eta = \eta_c$  is shown by the upper curve in Fig. 11. This corresponds to a discontinuous (first order) *intermediate wetting* transition from microscopic to mesoscopic films.

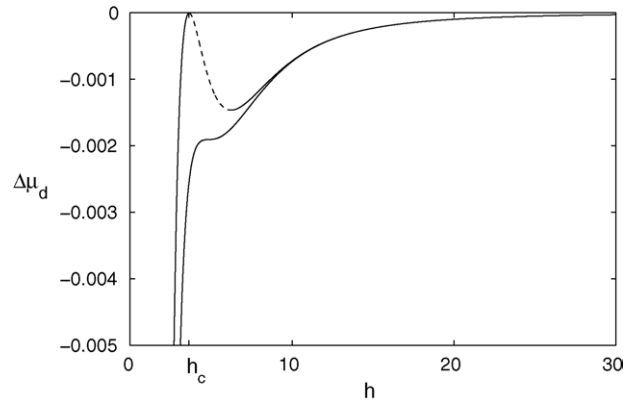


Fig. 11. The dependence of the dimensionless precursor layer thickness on the disjoining potential according to Eq. 26. The lower line ( $\eta = 0.00344$ ) corresponds to the continuous intermediate wetting transition. The upper line ( $\eta = \eta_c = 0.00407$ ) corresponds to onset of the frustrated complete wetting. The solid/dashed lines represent stable/unstable solutions, respectively. The parameters:  $\beta = 9$  and  $\chi = 0.4$ .

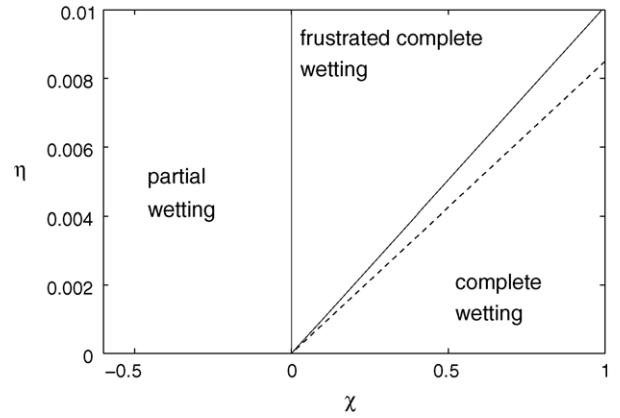


Fig. 12. The boundaries of wetting regions (solid line) in the parametric plane  $\chi - \eta$  for  $\beta = 9$  and at the equilibrium chemical potential  $\Delta\mu_d = 0$ . The dashed line depicts the continuous intermediate wetting transition at  $\Delta\mu_d < 0$ .

The lower curve with an inflection point in Fig. 11 corresponds to a continuous (second order) *intermediate wetting* transition, which is observed at a certain shifted value of chemical potential  $\Delta\mu_d < 0$ .

Fig. 12 summarizes these three transitions in the  $\chi - \eta$  plane. The critical point  $\chi = \eta = 0$  marks the *critical end point* [32] and corresponds to the sign change of the Hamaker constant; all three above wetting regions converge at the critical end point. Changing the inverse temperature  $\beta$  (for constant values of  $\eta$ ) does not change this picture in a qualitative way.

### 5. Discussion

In the current study, we have presented an analysis of wetting phenomena and interactions between liquid–vapor interfaces at microscopic, mesoscopic and macroscopic distances based on a relatively simple local density functional theory (DFT). The study is centered on computation of disjoining and conjoining potentials (which are important for dynamic computations). Focusing on the role of long-range van der Waals interactions, we

considered two models – hard wall and soft wall approximations – differing by the role of steric effects. The first difference corresponds to a precursor layer thickness and the quantitative form of the disjoining potential. Under similar external conditions, we found that droplets on smooth surfaces will roll-up before the ones on compliant surfaces [27,28] due to the steric forces. The distinct wall models also lead to a qualitatively different character of wetting transitions. A first order transition from partial to complete wetting occurs in the hard wall model only, turning to a second order transition in the soft wall model.

To capture a more realistic description of wetting transitions, we included a weak dependence on short-range polar interactions. Analytical derivation of the disjoining potential was carried out exploiting the sharp interface approximation, which showed a good agreement with a direct numerical solution of DFT Euler–Lagrange integral equations. We find that the qualitative nature of the sequence of wetting transitions stems from a competition between short- and long-scale interactions, best seen in the  $(\chi, \eta)$  parametric plane, while all other parameters, like temperature  $\beta^{-1}$  or short-range decay range  $\lambda$  have only a quantitative effect. The role of repulsive short-range interactions is analogous to steric effects, which are emphasized in the hard wall approximation. Thus, the presented simple model reproduces all major types of wetting transitions (between partial to complete/frustrating wetting and thin/thick precursor in coexistence with bulk fluid) of [14–16,32] as summarized in Fig. 12.

## Acknowledgements

This research has been supported by Israel Science Foundation and one of us (A. Y.) also acknowledges the support of Israel Council for Higher Education.

## References

- [1] L.M. Pismen, Y. Pomeau, Phys. Rev. E 62 (2000) 2480.
- [2] L.M. Pismen, Colloids Surf. A: Physicochem. Eng. Aspects 206 (2002) 11.
- [3] Y. Pomeau, C.R. Mecanique, 330 (2002) 207.
- [4] P.G. de Gennes, Rev. Mod. Phys. 57 (1985) 827.
- [5] L.M. Pismen, Y. Pomeau, Phys. Fluids 6 (2004) 2604.
- [6] C. Ebner, W.F. Saam, Phys. Rev. Lett. 38 (1977) 1486.
- [7] H. Nakanishi, M.E. Fisher, Phys. Rev. Lett. 49 (1982) 1565.
- [8] R. Lipowsky, D.M. Kroll, Phys. Rev. Lett. 52 (1984) 2303.
- [9] S. Dietrich, M. Schick, Phys. Rev. B 31 (1985) 4718.
- [10] J.E. Rutledge, P. Taborek, Phys. Rev. Lett. 69 (1992) 937.
- [11] D. Bonn, H. Kellay, G.H. Wegdam, Phys. Rev. Lett. 69 (1992) 1975.
- [12] H. Kellay, D. Bonn, J. Meunier, Phys. Rev. Lett. 71 (1993) 2607.
- [13] K. Ragil, J. Meunier, D. Broseta, J.O. Indekeu, D. Bonn, Phys. Rev. Lett. 77 (1996) 1532.
- [14] N. Shahidzadeh, D. Bonn, K. Ragil, D. Broseta, J. Meunier, Phys. Rev. Lett. 80 (1998) 3992.
- [15] D. Ross, D. Bonn, J. Meunier, Nature 400 (1999) 737.
- [16] D. Bonn, E. Bertrand, N. Shahidzadeh, K. Ragil, H.T. Dobbs, A.I. Posazhennikova, D. Broseta, J. Meunier, J.O. Indekeu, J. Phys.: Condens. Mater. 13 (2001) 4903.
- [17] B.V. Derjaguin, N.V. Churaev, V.M. Muller, Surface Forces, Consultants Bureau, New York, 1987.
- [18] A. Sharma, Langmuir 14 (1998) 4915.
- [19] U. Thiele, L. Bruschi, M. Bestehorn, M. Bär, Eur. Phys. J. E 11 (2003) 255.
- [20] L.M. Pismen, Phys. Rev. E 70 (2004) 51604.
- [21] J.D. van der Waals, J. Stat. Phys. 20 (1979) 197 (English translation: J.S. Rowlinson).
- [22] R. Evans, Adv. Phys. 28 (1979) 143.
- [23] S. Dietrich, M. Napiórkowski, Phys. Rev. A 43 (1991) 1861.
- [24] P. Tarazona, Phys. Rev. A 31 (1985) 2672; P. Tarazona, Phys. Rev. A 32 (1985) 3148.
- [25] Z. Tang, L.E. Scriven, H.T. Davis, J. Chem. Phys. 95 (1991) 2659.
- [26] A. González, M.M. Telo da Gama, Phys. Rev. E 62 (2000) 6571.
- [27] T. Onda, S. Shibuichi, N. Satoh, K. Tsujii, Langmuir 12 (1996) 2125.
- [28] G. McHale, N.J. Shirtcliffe, S. Aqil, C.C. Perry, M.I. Newton, Phys. Rev. Lett. 93 (2004) 036102.
- [29] L.D. Landau, E.M. Lifshitz, v. V, Statistical Physics, Part I, Pergamon Press, 1980.
- [30] L.M. Pismen, Phys. Rev. E 64 (2001) 021603.
- [31] J.R. Henderson, Z.A. Sabeur, J. Chem. Phys. 97 (1992) 6750.
- [32] S. Rafai, D. Bonn, E. Bertrand, J. Meunier, V.C. Weiss, J.O. Indekeu, Phys. Rev. Lett. 92 (2004) 245701.
- [33] R. Lipowsky, Phys. Rev. Lett. 52 (1984) 1429.
- [34] A. Sharma, Langmuir 9 (1993) 861; 3580.
- [35] A.J. Archer, R. Evans, J. Phys.: Condens. Mater. 14 (2002) 1131.